HHS Public Access

Author manuscript

Nat Methods. Author manuscript; available in PMC 2014 August 01.

Published in final edited form as:

Nat Methods. 2013 October ; 10(10): 1003–1005. doi:10.1038/nmeth.2633.

Absolute quantification by droplet digital PCR versus analog real-time PCR

Christopher M Hindson[1,6,7], **John R Chevillet**[2,7], **Hilary A Briggs**[2], **Emily N Gallichotte**[2], **Ingrid K Ruf**[2], **Benjamin J Hindson**[1,6], **Robert L Vessella**[3], and **Muneesh Tewari**[2,4,5]

[1]Digital Biology Center, Bio-Rad Laboratories, Inc., Pleasanton, California, USA

[2]Division of Human Biology, Fred Hutchinson Cancer Research Center, Seattle, Washington, USA

[3]Department of Urology, University of Washington, Seattle, Seattle, Washington, USA

[4]Division of Clinical Research, Fred Hutchinson Cancer Research Center, Seattle, Washington, USA

[5]Division of Public Health Sciences, Fred Hutchinson Cancer Research Center, Seattle, Washington, USA

Abstract

Nanoliter-sized droplet technology paired with digital PCR (ddPCR) holds promise for highly precise, absolute nucleic acid quantification. Our comparison of microRNA quantification by ddPCR and real-time PCR revealed greater precision (coefficients of variation decreased by 37–86%) and improved day-to-day reproducibility (by a factor of seven) of ddPCR but with comparable sensitivity. When we applied ddPCR to serum microRNA biomarker analysis, this translated to superior diagnostic performance for identifying individuals with cancer.

Traditional digital PCR[1] is a method of absolute nucleic acid quantification based on the partitioning of individual analyte molecules into many replicate reactions at limiting

Correspondence should be addressed to M.T. (mtewari@fhcrc.org).
[6]Present address: 10X Technologies, Pleasanton, California, USA
[7]These authors contributed equally to this work

Note: Any Supplementary Information and Source Data files are available in the online version of the paper

Author Contributions: C.M.H. designed experiments, performed experiments, and analyzed and interpreted data. J.R.C. designed the data analysis plan, analyzed and interpreted data, and managed the specimen set. H.B. performed experiments and interpreted data. E.G. performed experiments and interpreted data. I.K.R. contributed to initial design of experiments and project management. B.J.H. designed experiments and interpreted data. R.L.V. was responsible for design, collection and quality control of the case-control clinical specimen cohort. M.T. conceived and supervised the study, designed experiments, and interpreted data. The manuscript was written mainly by J.R.C., with contributions from C.M.H. and M.T. All authors reviewed and provided editorial comments on the manuscript.

Competing Financial Interests: The authors declare competing financial interests: details are available in the online version of the paper. “C.M.H. and B.J.H. were formerly employees of Quantalife, Inc. and Bio-Rad, Inc., including during periods that the work was done. M.T.'s laboratory received some consumable supplies from Quantalife, Inc. and Bio-Rad, lnc. during the course of the studies. M.T. is an inventor on patent application US 12/993,828 pertaining to extracellular microRNA biomarkers.”

dilution, resulting in one or zero molecules in most reactions. After endpoint PCR, the starting concentration of template is determined by Poisson statistical analysis of the number of positive (containing amplified target) and negative (no amplified target detected reactions. The digital PCR concept[2] has many potential advantages over real-time PCR, including the capability to obtain absolute quantification without external references and robustness to variations in PCR efficiency[3]. Recently, technology has become commercially available that permits reactions to be partitioned into nanoliter-sized, aqueous droplets in oil rather than multiwell plates. Rapid microfluidic analysis of thousands of droplets per sample[4,5] makes ddPCR practical for routine use. In addition, the practical dynamic range of the system is substantially improved by using highly uniform droplets, which (with Poisson correction for multiple target molecules per droplet) enable the precise calculation of concentrations even above conditions of limiting dilution[4,5].

Data regarding the empirical operating characteristics of ddPCR versus real-time PCR including technical precision, sensitivity, accuracy and day-to-day reproducibility are scant. A recent study had suggested comparable performance of the two methods but was limited to a single target in one background matrix and revealed contradictory performance in analyses of laboratory standards versus clinical specimens[6]. Here we report a systematic comparison of ddPCR and real-time PCR performance, using a range of synthetic targets, different background matrices, as well as low-target-abundance biological samples. We focused on the quantification of cDNAs corresponding to microRNAs (miRNAs), which are small regulatory RNA molecules with diverse cellular functions[7]. miRNAs also exist in highly stable extracellular forms in the vascular circulation[8,9] with potential hormonal function[10] and can be useful as blood-based biomarkers for cancer[8] and other diseases[11].

We used serial dilutions of synthetic oligoribonucleotides (Supplementary Fig. 1 and Supplementary Table 1) representing six different mature human miRNAs: miR-141, miR-375, miR-210 (circulating miRNA cancer biomarkers[8,12,13]), miR-135b, miR-205 (tissue-based cancer biomarkers[14,15]) and miR-16 as a broadly expressed control. To assess variation at different stages of the procedure (preparation of serial dilution, reverse transcription (RT) and PCR), we used a hierarchical experimental design of nested replicates (Supplementary Fig. 1). For each miRNA, we prepared a twofold dilution series and reverse-transcribed it in triplicate. We analyzed each RT reaction in triplicate by ddPCR and real-time PCR, using aliquots of the same PCR reaction mixture. We replicated this entire workflow in triplicate, with individual dilution series replicates prepared on different days. Furthermore, we prepared each dilution series using, in parallel, water and plasma RNA from a healthy donor in solution as diluents, to determine performance in the setting of pure template as well as in a complex background matrix.

In the water matrix, ddPCR reduced mean coefficients of variation (CVs) 37–86% compared to real-time PCR with respect to overall variation (Fig. 1a,b) and 48–72% with respect to PCR-specific variation (Supplementary Table 2). ddPCR consistently displayed lower variation than real-time PCR for all miRNAs tested, in both matrices (Fig. 1a and Supplementary Fig. 2) and whether calculated across PCR replicates, RT replicates or serial dilution preparation replicates (Supplementary Figs. 3–6, and Supplementary Tables 2 and 3). However, ddPCR was not uniformly more sensitive compared to real-time PCR across

the six microRNAs examined (Supplementary Tables 4 and 5). As an additional performance metric that cannot be examined using real-time PCR, we noted that absolute measurements by ddPCR corresponded to 49–114% of the theoretically input copies (Supplementary Table 6), indicating that absolute detection by ddPCR is remarkably efficient.

To compare the diagnostic sensitivity and specificity of ddPCR versus real-time PCR on clinical serum samples, we collected sera from 20 patients with advanced prostate cancer and from 20 age-matched, healthy male controls, and measured the abundance of miR-141, which has been shown to be elevated in the serum of patients with advanced prostate cancer[8,12]. We analyzed aliquots of cDNA corresponding to the serum RNA samples using our ddPCR workflow and, in parallel, a current standard real-time PCR method widely used for serum miRNA biomarker analysis[16], in triplicate on three different days (Fig. 2a and Supplementary Fig. 7). We also analyzed aliquots of the ddPCR master mix for each reaction in parallel by real-time PCR (Fig. 2a), in similar fashion to the previous experiments analyzing synthetic miRNAs. In the analysis of synthetic miR-141 standard curves run in parallel, ddPCR showed greater precision (Supplementary Fig. 8) but was not more sensitive (Supplementary Table 7), consistent with the results presented above (Fig. 1 and Supplementary Tables 2 and 4).

Absolute quantification by ddPCR reduced variation in measurement of miR-141 in clinical serum samples by an average factor of seven relative to standard real-time PCR (Fig. 2b, and Supplementary Tables 8 and 9). Although all three methods detected higher average miR-141 abundance in the serum RNA of cases (prostate cancer patients) than in controls, ddPCR better resolved cases from controls (Fig. 2c), and in a nonparametric analysis, the difference reached statistical significance (Mann-Whitney test, $P = 0.0036$), whereas statistical significance was not reached in a real-time PCR analysis of the ddPCR mixture ($P = 0.1017$) or standard real-time PCR in this sample set ($P = 0.1199$). Receiver operating characteristic (ROC) analysis revealed that ddPCR more accurately classified case versus control specimens (Fig. 2d), as reflected by an increased area under a ROC curve (AUC of 0.770 for ddPCR versus AUC of 0.653 for the ddPCR mixture analyzed by real-time PCR and AUC of 0.645 for standard real-time PCR).

We speculate that ddPCR may also be more resilient to differences in sample quality; by virtue of being an end-point approach, it is more tolerant to PCR inhibitors, which affect amplification efficiency. Furthermore, although our study focused on cDNAs reverse-transcribed from miRNAs, it fundamentally represents a characterization of the empirical operating characteristics of ddPCR versus real-time PCR and should be relevant to a broad variety of applications where high-performance quantification of nucleic acid targets is required.

Online Methods

General procedure for generation of miRNA standard curves

Six RNase-free, HPLC-purified 5′-phosphorylated miRNA oligoribonucleotides were synthesized (Integrated DNA Technologies) for the analytical portion of this study,

corresponding to hsa-miR-16 (5′-phospho-UAGCAGCACGUAAAUAUUGGCG-OH-3′), hsa-miR-141 (5′-phospho-UAACACUGUCUGGUAAAGAUGG-OH-3′), hsa-miR-135b (5′-phospho-UAUGGCUUUUCAUUCCUAUGUGA-OH-3′), hsa-miR-205 (5′-phospho-UCCUUCAUUCCACCGGAGUCUG-OH-3′), hsa-miR-210 (5′-phospho-CUGUGCGUGUGACAGCGGCUGA-OH-3′) and hsa-miR-375 (5′-phospho-UUUGUUCGUUCGGCUCGCGUGA-OH-3′). Stock solutions of 10 μM synthetic oligonucleotide in RNase-free/DNase-free water were prepared according to the concentrations and sample purity quoted by the manufacturer (based on spectrophotometry analysis). To minimize uncertainty resulting from pipetting, all dilutions where the volumetric dilution factor exceeded 2× (see Supplementary Table 1, dilutions 1–4) were performed on an analytical balance, such that the predicted copies going into the standard curves could be accurately[5] scaled using a gravimetric dilution factor. All further dilutions for the standard curve (Supplementary Table 1, dilutions 5–11) were performed volumetrically. Approximately 5–5,000 copies per 20 μl PCR reaction with nine intermediate twofold serial dilutions and additional no template controls (NTCs; zero copies) were examined. Dilution series for each of the synthetic miRNAs were made in either RNase/DNase-free H_2O or in healthy human donor plasma RNA solution to provide a constant background of endogenous miRNAs. Our modified procedure used for isolating miRNAs from plasma with miRNeasy kits (Qiagen) has been described previously[16]. To ensure a homogenous plasma RNA solution for use as diluent, multiple plasma RNA extraction batches collected using this protocol[16] were pooled and mixed by gentle pipetting, then divided into 60-μl aliquots and stored at −80 °C until use. All experiments for this work were conducted at the Fred Hutchinson Cancer Research Center.

Procedure for reverse transcription–ddPCR and reverse transcription–real-time-PCR

RT of input miRNAs (Supplementary Table 1, dilutions 5–11) was conducted using reagents from the TaqMan miRNA Reverse Transcription Kit and 60× target-specific RT primers (both from Applied BioSystems, Inc.). The kit contains the following components that, together with the stem-loop primers and RNase/DNase-free H_2O, comprise what is forthwith referred to as ‘RT mix’ (numbers in parentheses are final volumes in a 10-μl RT reaction containing 8 μl RT mix): 10× RT buffer (1 μl), RNase inhibitor (0.12 μl), 100 mM each dNTP (0.1 μl), Multiscribe reverse transcriptase (0.66 μl), 60× RT primer (0.17 μl), RNase/DNase-free H_2O (5.95 μl). The volumetric ratio of RT mix to input miRNA solution was 4:1, and triplicate 10 μl RT reactions (Supplementary Fig. 1) for each point of the curves were taken from a corresponding well-mixed stock solution of a given concentration (34 μl total volume; 7 μl input miRNA). The reverse transcription thermal-cycling procedure for triplicate 10 μl RTs used holds at 16 °C for 30 min, then 42 °C for 30 min and 85 °C for 5 min (Tetrad2 Peltier Thermal Cycler; Bio-Rad). 7 μl of RT product for each concentration was thoroughly mixed by pipette resuspension with 133 μl solutions containing Master Mix (Bio-Rad, 70 μl of 2× mix), the target-specific TaqMan Real Time PCR primer probe set (Applied Biosystems, 2.33 μl of 60× solution) and RNase/DNase-free H_2O (60.67 μl). From this bulk solution, triplicate PCR reactions were carried out using both ddPCR (20 μl PCR reaction) and real-time PCR (5 μl PCR reaction), such that both ddPCR and real-time PCR reactions had identical concentrations of synthetic miRNA oligonucleotides. Real-time PCR experiments were performed on an Applied Biosystems Viia 7 instrument with the following

thermal-cycling procedure; 95 °C for 10 min, followed by 40 cycles of 95 °C for 15 s and 60 °C for 1 min (1.6 °C/s ramp rate) as specified in the TaqMan MicroRNA Assay protocol provided by the manufacturer (Applied Biosystems).

To provide the best possible analysis of the raw real-time PCR data for comparison to ddPCR, real-time PCR data collected in this manner were analyzed with the Viia 7 instrument software v1.0 using three separate conventional approaches[3,17] and compared side by side to deduce which method gave the lowest variability (data not shown). When using the first method, we examined the effect of using a universal baseline and threshold to aid data consistency across the study. The baseline was set between 8 cycles and 20 cycles (to base this on the background signal found in early cycles of amplification) with a manual fluorescence threshold of 20,000 Relative Fluorescence Units (RFUs) with ROX (carboxy-x-rhodamine passive reference dye) normalization disabled (ddPCR master mix does not contain ROX dye). In the second method, the threshold was manually set by the operator to exclude spurious noise and intersect the exponential amplification portion of the fluorescence curve as centrally as possible. ROX normalization was disabled. The third method used the Viia 7 signal processing algorithm to automatically call baseline and threshold, with ROX normalization disabled. Method 3 was found to give the lowest variability between PCRs, and therefore this method was used for analysis of all data derived from real-time PCR analysis of ddPCR reaction mixtures. Note that data derived from the standard real-time PCR protocol (i.e., used to analyze clinical specimens) was analyzed using its corresponding data analysis procedure[8], which was identical to method 3 above with the exception of inclusion of ROX normalization. Curves that did not show typical exponential amplification morphology were included in the presentation of the whole data (Fig. 1a and Supplementary Fig. 2) but were excluded from subsequent summary operating characteristic and statistical analysis (Supplementary Figs. 3–6 and Supplementary Tables 2–5) to provide the best possible estimate of real-time PCR performance. Undetermined cycle thresholds were arbitrarily set to 40 as a limiting estimate of the maximum possible abundance of target. Target abundance relative to the mean of highest concentration tested was determined by Pfaffl analysis of the cycle-threshold (Ct) data[18], using the empirically determined PCR efficiency for each miRNA. In the case of the standard curves generated for the analysis of clinical specimens, results are presented as the mean of real-time PCR triplicates.

Limit of quantification (LOQ) was defined as the lowest concentration tested that remained above or equal to the lower limit of linear range of the assay (LLLR) and above or equal to the limit of detection (LOD). Linear range was determined by runs-testing[19], removing successive dilution points until the P value was >0.05, indicating no significant deviation from linearity (Prism Version 5.0c software). LOD was defined as $\langle x \rangle_{bi} + k s_{bi}$, where $\langle x \rangle_{bi}$ equals the mean of the no-template controls, s_{bi} is s.d. of no-template controls, and $k = 2.479$ (99% confidence interval)[20].

The ddPCR system, workflow, operating characteristics and analytical performance has been recently described in detail by some of the authors of this paper in two recent publications[4,5], but a brief summary of this technology follows. At the start of these studies, the instrument and reagents used were manufactured by Quantalife, Inc., which was

subsequently acquired by Bio-Rad, Inc., which is the current manufacturer and distributor. Each 20 μl PCR reaction (see above) was loaded into an 8-channel, single-use consumable droplet generation cartridge. 60 μl of oil containing emulsion-stabilizing, biocompatible surfactant was loaded into adjacent oil wells, and the microfluidic chip was loaded into a beta-series prototype droplet generator (DG). The DG applies a vacuum to the outlet well creating a pressure difference across the cartridge that simultaneously partitions the sample present in each of the 8 wells into ∼20,000 monodisperse droplets of accurately known volume. This process occurs at a rate of ∼1,000 droplets/s per well. The resulting water-in-oil emulsions were pipette-transferred from the outlet well to a 96-well polypropylene plate (Eppendorf), sealed with foil and then amplified to endpoint using a Tetrad2 Peltier Thermal Cycler (Bio-Rad) and the cycling protocol: 95 °C for 10 min then 40 cycles of 95 °C for 15 s and 60 °C for 1 min (2.5 °C/s ramp rate) with a final 10 min hold at 98 °C. Plates containing amplified droplets were loaded into an early-access, beta-version of the commercially available QX100 droplet reader (Bio-Rad), which aspirates droplets from the 96-well plate, one well at a time, and streams them single-file (∼1,500 droplets/s) past a two-color FAM/VIC (FAM and VIC fluorescence dyes, Life Technologies Corp.) detector sampling at 100 kHz. Discrimination between droplets that did not contain target (negatives) and those that did (positives) was achieved by applying a global fluorescence amplitude threshold. For all of the miRNA assays, the global fluorescence threshold was set at 4,000 relative fluorescence units (RFUs) regardless of the assay efficiency. Concentration estimates (λ) were based on the fraction of droplets where amplification has occurred (*p*) modeled as a Poisson distribution (equation (1)).

$$\lambda = -\ln(1-p) \quad (1)$$

Because each droplet is an independent PCR reaction vessel of equal and defined volume, the droplets of technical replicates (triplicate wells) can be pooled to create a ‘metawell’. To compute total ± 95% confidence intervals about concentration estimates of metawells (comprised of previously described[21,22] Poisson ± 95% CIs and ‘real world error’; concentration differences between wells) we applied the following meta-analysis techniques. Given *k* replicates with concentrations m_1, m_2, … m_k and Poisson variances v_1, v_2, … v_k, respectively, we define the weight (*w*) of replicate *i* as reciprocal of its variance as

$$w_i = \frac{1}{v_i} \quad (2)$$

Let $\overline{m}$ be the weighted average of concentrations and consider the following random variable that measures fluctuation of concentrations around this weighted mean:

$$T = \sum_{i=1}^{k} w_i (m_i - \overline{m})^2 \quad (3)$$

This is the sum of squares of approximately standard normal random variables and can therefore be approximated as a chi-squared distribution. The mean of the distribution is the number of degrees of freedom ($df = k - 1$). If *T* is less than *df*, we say that there is no

additional real-world variance. If *T* is more than *df*, then it suggests there is additional real-world variance $r = T - df$. As *T* is based on standard normal variables, we scale back r to r′ in original units after applying an appropriate correction factor:

$$r' = \frac{r}{\sum w_i - \frac{\sum w_i^2}{\sum w_i}} \quad (4)$$

We can add r' to Poisson variance to give total variance for each replicate. We redefine the weight of each replicate as:

$$w_i = \frac{1}{v_i + r'} \quad (5)$$

from which we can compute the total uncertainty around the metawell as

$$v = \frac{1}{\sum w_i}. \quad (6)$$

The final estimate *m* ī̄s recomputed as weighted average of concentrations with new weights. By setting r' to 0, we will get estimate of *v* in presence of only Poisson error. This meta-analysis is a statistically rigorous method to test the existence of real-world error in a group of replicate droplet digital PCR wells (US Patent Application 20130017551). All of these data-analysis methods are implemented in the Quantasoft (1.1.1.0) data analysis package, installed with the droplet reader.

Procedure for the quantitation of miR-141 in clinical specimens

Human serum samples from individuals with metastatic prostate cancer and prostate-cancer–negative controls were collected after written informed consent was obtained. All participants signed a University of Washington Human Subjects Committee approved Informed Consent Form for a peripheral blood draw and the research was approved and supervised by the University of Washington and Fred Hutchinson Cancer Research Center Institutional Review Boards. Prostate-cancer–negative donors were recruited among individuals undergoing screening for prostate cancer and found to be negative by digital-rectal examination (DRE) and serum PSA analysis. Individuals with metastatic prostate cancer were recruited among previously diagnosed patients undergoing treatment at the University of Washington (Seattle). Procedures for sample collection, pretreatment and RNA extraction have been described previously[16]. The same protocol was adopted here without modification. In this study, a smaller cohort of clinical specimens corresponding to $n = 20$ advanced prostate cancer cases and $n = 20$ healthy controls was analyzed (previously, $n = 25$ each group). The patient specimens studied here were distinct from (not a subset of) those we studied previously[8]. Using the population-variance data from the previous study, we performed a power calculation and determined that $n = 12$ individuals per group would result in 81% power to detect a difference in means of fourfold (alpha = 0.05, two tails). We chose to analyze specimens from $n = 20$ individuals per group, as this was above the

minimum predicted by the power calculation, feasible and simplified the technical work relative to the previous study. The experimenter was kept blinded to case status (i.e., cancer versus control).

For comparing the performance of ddPCR to real-time PCR in the clinical specimens, we used the standard real-time PCR method that we previously described[16]. Synthetic miR-141 standard curves used in this portion of the study were made using MS2 carrier RNA, which leads to improved circulating miRNA precision in real-time PCR analyses[23] and therefore was included to provide the best possible real-time PCR performance to compare with ddPCR. ddPCR showed superior precision (Supplementary Fig. 8), consistent with our results displayed in Figure 1a,b and comparable limits of quantification (Supplementary Table 7) for miR-141 in the analyses of these standard curves. Owing to limited serum RNA volume for the large number of replicates needed for this study, we diluted the initial serum RNA specimens by a factor of 1.5. To allow a direct comparison of performance between ddPCR (which uses Bio-Rad ddPCR Supermix for Probes, 186-3010) and standard circulating miRNA real-time PCR (which uses ABI Taqman Universal PCR MasterMix no UNG, 4326614), differences in the reagent volumes used between the Bio-Rad ddPCR and the standard circulating miRNA real-time PCR protocols needed to be accommodated to achieve the same concentration of cDNA in each comparable reaction across the methods (Supplementary Fig. 7). As a result of these necessary adjustments, the concentration of input cDNA analyzed per reaction for both ddPCR and real-time PCR methods was ultimately about tenfold lower than that used previously[8]. After reverse transcription, the cDNAs corresponding to the sets of standard curves (Supplementary Fig. 8) and the 40 clinical specimens (Fig. 2) were each split into six aliquots for subsequent PCR reactions (see below). Three of these six cDNA aliquots were added to ABI master mix for subsequent real-time PCR, and the remaining three were added to Bio-Rad mastermix to conduct ddPCR and real-time PCR (Fig. 2). The prepared 100 μl ddPCR master mix for each sample was divided into three 20 μl aliquots for analysis by ddPCR and three 5 μl aliquots for analysis by real-time PCR. The prepared 20 μl standard real-time PCR master mix for each sample was divided into 3 × 5 μl aliquots for analysis by real-time PCR (Fig. 2 and Supplementary Fig. 7). For the analysis of clinical specimens, ddPCR triplicates were combined into a single metawell before Poisson analysis and recovery correction by *Caenorhabditis elegans* recovery-yield miRNA spike-ins[16]. For real-time PCR, the concentration of analyte was calculated by Ct comparison to the standard curve, and results were presented as the mean of the PCR triplicates corrected by *C. elegans* spike-ins[16]. Statistical significance was determined by Mann-Whitney analysis (95% confidence intervals, two tails) and receiver operating characteristic (ROC) analysis was performed using Prism 5.0c software.

Supplementary Material

Refer to Web version on PubMed Central for supplementary material.

Acknowledgments

We thank G. Karlin-Neumann, G. McDermott and C. Pritchard for advice during the course of these studies, R. Parkin, J. Noteboom and D. Gonzales for technical assistance, and the volunteers who provided blood specimens

for analysis in this study. This work was supported by a Canary Foundation–American Cancer Society Postdoctoral Fellowship in the Early Detection of Cancer (PFTED-09-249-01-SEID to J.R.C.), grant R01EB010106 from the US National Institute of Biomedical Imaging and Bioengineering (to B.J.H.), PO1 grant CA-85859 (to R.L.V.) and the Pacific Northwest Prostate Cancer Specialized Program of Research Excellence (SPORE) grant P50-CA-097186 (to R.L.V.). M.T. acknowledges generous support from a Damon Runyon-Rachleff Innovation Award; US National Institutes of Health Transformative R01 grant R01DK085714; National Cancer Institute (NCI) grant P50 CA83636 from the Pacific Ovarian Cancer Research Consortium Specialized Program of Research Excellence (SPORE) in Ovarian Cancer; grant U01 CA157703, which is part of the NCI's Strategic Partnerships to Evaluate Cancer Signatures II (SPECS II) program; Department of Defense Ovarian Cancer Career Development Award (OC080159) and Peer-Reviewed Cancer Research Program Award CA100606; Stand Up To Cancer Innovative Research Grant SU2C-AACR-IRG1109; and funding from the Canary Foundation.

References

1. Vogelstein B, Kinzler KW. Proc Natl Acad Sci USA. 1999; 96:9236–9241. [PubMed: 10430926]
2. Sykes PJ, et al. Biotechniques. 1992; 13:444–449. [PubMed: 1389177]
3. Bustin SA, Nolan T. J Biomol Tech. 2004; 15:155–166. [PubMed: 15331581]
4. Hindson BJ, et al. Anal Chem. 2011; 83:8604–8610. [PubMed: 22035192]
5. Pinheiro LB, et al. Anal Chem. 2012; 84:1003–1011. [PubMed: 22122760]
6. Hayden RT, et al. J Clin Microbiol. 2013; 51:540–546. [PubMed: 23224089]
7. Kloosterman WP, Plasterk RH. Dev Cell. 2006; 11:441–450. [PubMed: 17011485]
8. Mitchell PS, et al. Proc Natl Acad Sci USA. 2008; 105:10513–10518. [PubMed: 18663219]
9. Arroyo JD, et al. Proc Natl Acad Sci USA. 2011; 108:5003–5008. [PubMed: 21383194]
10. Redis RS, Calin S, Yang Y, You MJ, Calin GA. Pharmacol Ther. 2012; 136:169–174. [PubMed: 22903157]
11. Reid G, Kirschner MB, van Zandwijk N. Crit Rev Oncol Hematol. 2011; 80:193–208. [PubMed: 21145252]
12. Bryant RJ, et al. Br J Cancer. 2012; 106:768–774. [PubMed: 22240788]
13. Lawrie CH, et al. Br J Haematol. 2008; 141:672–675. [PubMed: 18318758]
14. Munding JB, et al. Int J Cancer. 2012; 131:E86–E95. [PubMed: 21953293]
15. du Rieu MC, et al. Clin Chem. 2010; 56:603–612. [PubMed: 20093556]
16. Kroh EM, Parkin RK, Mitchell PS, Tewari M. Methods. 2010; 50:298–301. [PubMed: 20146939]
17. Nolan T, Hands RE, Bustin SA. Nat Protoc. 2006; 1:1559–1582. [PubMed: 17406449]
18. Pfaffl MW. Nucleic Acids Res. 2001; 29:e45. [PubMed: 11328886]
19. Massart, DL. Handbook of chemometrics and qualimetrics. Elsevier; 1997.
20. McNaught, AD.; Wilkinson, A. International Union of Pure and Applied Chemistry. Compendium of chemical terminology: IUPAC recommendations. 2nd. Blackwell Science; 1997.
21. Weaver S, et al. Methods. 2010; 50:271–276. [PubMed: 20079846]
22. Dube S, Qin J, Ramakrishnan R. PLoS ONE. 2008; 3:e2876. [PubMed: 18682853]
23. Andreasen D, et al. Methods. 2010; 50:S6–S9. [PubMed: 20215018]

a

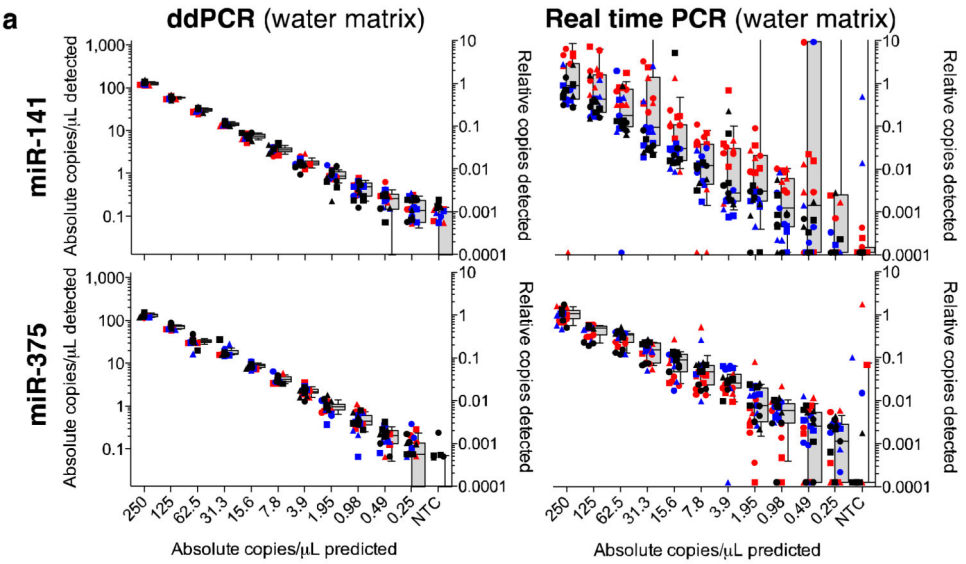

b

	Mean reduction in coefficient of variation (%)			
	Across preparative replicates		Across PCR replicates	
miRNA	Water matrix	Plasma RNA matrix	Water matrix	Plasma RNA matrix
miR-141	86	74	72	77
miR-375	62	64	50	49
miR-210	37	64	48	67
miR-135b	81	81	68	72
miR-205	52	78	59	72
miR-16	54	NA*	65	NA*

Figure 1.

Quantification of synthetic miRNA oligonucleotides by ddPCR and real-time PCR. (**a**) Comparative analysis of dilution series of indicated miRNAs in water. Each color represents one preparative (independent preparation of a dilution series) replicate and each shape represents individual RTs. (RT 1, circle; RT 2, square; and RT 3, triangle). Box and whisker plots (gray) show median (center line), 25th and 75th percentiles (box), and 10th and 90th percentiles (whiskers). NTC: No Template Control. (**b**) Reduction in CV, measured as $(CV_{\text{real-time PCR}} - CV_{\text{ddPCR}})/(CV_{\text{real-time PCR}})$. *, endogenous abundance of miR-16 in plasma RNA was higher than the maximum concentration of synthetic oligonucleotide examined.

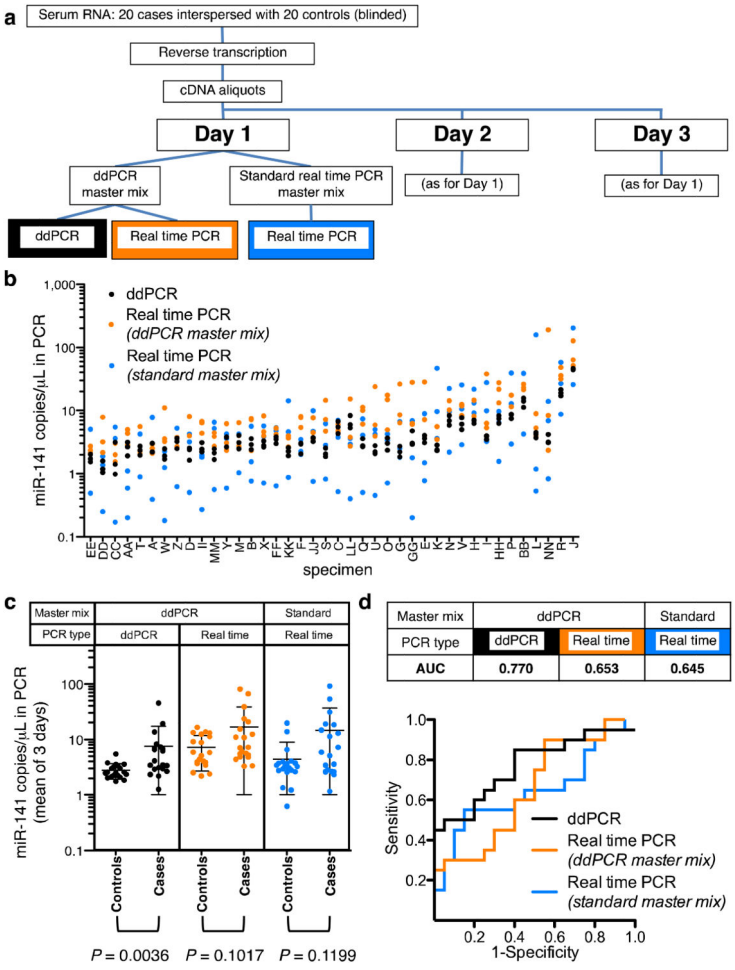

Figure 2.

Quantification of circulating miRNA biomarker in clinical serum samples by ddPCR and real-time PCR. (**a**) Workflow used to measure the abundance of a circulating miRNA biomarker in clinical samples. (**b**) Replicate analyses of serum-derived miR-141 over 3 d. Data represent metawell analysis of three ddPCR replicates per day or the means of three real-time PCR replicates per day (individuals are sorted on the *x*-axis by mean abundance of ddPCR values). See Supplementary Data for key to specimen identifiers. (**c**) Data from **b** presented as the means of results over 3 d for cases and controls. Over the dot plots, central lines indicate the mean; error bars, s.d. ($n = 20$) *P* values: Mann-Whitney test, two-tailed. (**d**) ROC curve analysis of data in **c**.